Influence of the Au/Ag Ratio on the Catalytic Activity of Dendrimer-Encapsulated Bimetallic Nanoparticles in Microreactors

Roberto Ricciardi, Jurriaan Huskens and Willem Verboom*

Laboratory of Molecular Nanofabrication, MESA+ Institute for Nanotechnology, University of Twente, P.O. Box 217, 7500 AE, Enschede, The Netherlands

Received: 04 May 2015; accepted: 28 May 2015

Dendrimer-encapsulated Au/Ag alloy nanoparticles (Au/Ag DENs) were covalently attached to a monolayer-functionalized inner surface of glass microreactors. The influence of the bimetallic alloy structure and of the different metal ratios was investigated for the reduction of 4-nitrophenol using $NaBH_4$. The Au/Ag–dendrimer nanocomposite with a 1:1 Au/Ag metal ratio showed the highest activity as compared to other metal ratios and to pure Ag and Au. The dendrimer template exerted a stabilizing effect for six consecutive days of use with almost no decrease in conversion. This strategy enables the screening and investigation of a variety of bimetallic nanocatalysts in continuous-flow microreactors.

Keywords: flow microreactors, nanoparticles, heterogeneous catalysis, reductions, nanoalloys

1. Introduction

Bimetallic nanoparticles (NPs) are receiving increasing attention because of the advantageous features of combining two or more metals in the same heterocomposite structure, with widespread application in the biomedical, electronic, and catalytic areas [1]. Following the increasing importance of nanotechnology in catalysis [2], especially in terms of lower environmental impact of chemical reactions [3], bimetallic particles in the range of a few nanometers are one of the major candidates in heterogeneous catalysis [4]. Due to synergistic effects, both geometric and electronic, the physical and chemical behavior of a bimetallic system is considerably different from the mere combination of the two metal constituents [5]. Therefore, the catalytic activity can be tailored by combining two or more metals in the same nanocomposite structure [6].

Undoubtedly, the surface properties of heterometallic nanocomposites rely on the morphology, size, and distribution of the nanoparticles. These properties can be altered in case of supported NPs [4b], despite the tremendous progress achieved in recent years in the synthesis of heterogeneous monometallic species [7]. To overcome this drawback, dendrimers offer the opportunity to synthesize well-defined metallic NPs and to combine the advantages of homogeneous and heterogeneous catalysis [8]. The synthesis of bimetallic dendrimer-encapsulated NPs (DENs) usually follows one of three main approaches: cocomplexation, sequential loading, and partial displacement [9]. Alloy DENs are usually formed via the cocomplexation route, where the two metal salts are added at the same time and upon metal ion–dendrimer complexation, a strong reducing agent (usually $NaBH_4$) yields well-mixed alloy NPs [10].

Despite the increasing importance of nanocatalysis within continuous-flow microreactors [11], there are relatively few examples of supported bimetallic nanocatalysts in combination with microfluidic reactors [12]. However, the large surface-to-volume ratio and the improved heat and mixing efficiency ensured by microstructured reactors are expected to be beneficial to fully exploit the synergistic properties of supported bimetallic NPs. The advantages of flow microreactors in chemical synthesis and catalysis are summarized in some recent excellent reviews [13]. Recently, we presented a strategy for the covalent anchoring of poly(amidoamine) (PAMAM) dendrimers within flow microreactors for the preparation of well-defined Pd DENs [14]. The good catalytic performance of these catalysts was demonstrated for C–C cross-coupling reactions [15].

Herein, DENs covalently attached within flow microreactors were used to investigate the influence of the metal composition on the catalytic activity of Au/Ag alloy nanocomposites. The reduction of 4-nitrophenol represents a benchmark reaction for the study of the catalytic activity of metallic NPs and was chosen as model reaction. The benefits, in terms of screening of the optimal metal composition and the catalytic activity and stability, of the combination of bimetallic DENs and continuous-flow will be clearly demonstrated.

2. Results and Discussion

2.1. Flat Surface and Microreactor Functionalization. Gold/silver alloy DENs were formed by encapsulation within the generation 4 of PAMAM dendrimers (G4-NH_2) following the cocomplexation approach. These DENs were attached to the inner walls of flow microreactors based on a recent procedure developed in our group (Scheme 1) [14]. To this end, the inner surface of a glass microreactor was first modified with a reactive monolayer of (3-aminopropyl)triethoxysilane (APTES) followed by *p*-phenylene diisothiocyanate (DITC). In this way, the exposed isothiocyanate groups were used for the covalent anchoring of G4-NH_2 dendrimers via formation of thiourea bonds [16]. Different mixtures of $HAuCl_4$ and $AgNO_3$ salts with G4-NH_2 dendrimers were prepared, namely, Au/Ag 1:0, 3:1, 1:1, 1:3, and 0:1 [17], followed by $NaBH_4$ reduction.

The ultraviolet–visible (UV–vis) spectra of different G4-NH_2 bimetallic nanocomposites were characterized by the presence of only one surface plasmon resonance (SPR) band in the region between 400 and 500 nm, suggesting the formation of alloy NPs (Figure S1). In fact, previous studies have shown that Au/Ag alloys exhibit a single peak in their absorption spectra, the position of which shifts gradually from that of pure Ag at around 400 nm to that of pure Au at around 500 nm [17, 18]. This observation indicates that the NPs are alloys rather than core–shell particles or mixtures of monometallic NPs, in which case, the UV–vis spectrum would show two different peaks corresponding to Ag and Au [18a, 19]. Transmission electron microscopy (TEM) images of a 1:1 Au/Ag alloy NPs sample showed uniform spherical NPs with an average diameter of 3.2 ± 0.8 nm (Figure 1). The obtained average size is in agreement with the study of Endo et al. [17] for Au/Ag DEN nanocomposites. While pure gold NPs exhibit a similar size as the bimetallic ones, pure silver NPs have been shown to display a bigger diameter (around 10 nm) [17, 19]. Therefore, the formation of quite monodispersed NPs supports alloy formation [20].

Figure 2a shows a high-resolution TEM (HRTEM) image of the alloy nanoparticles and their electron diffraction patterns. A basal

* Author for correspondence:w.verboom@utwente.nl

DOI: 10.1556/1846.2015.00018

First published online: 16 July 2015

Scheme 1. Microreactor surface functionalization with dendrimer-encapsulated Au/Ag NPs

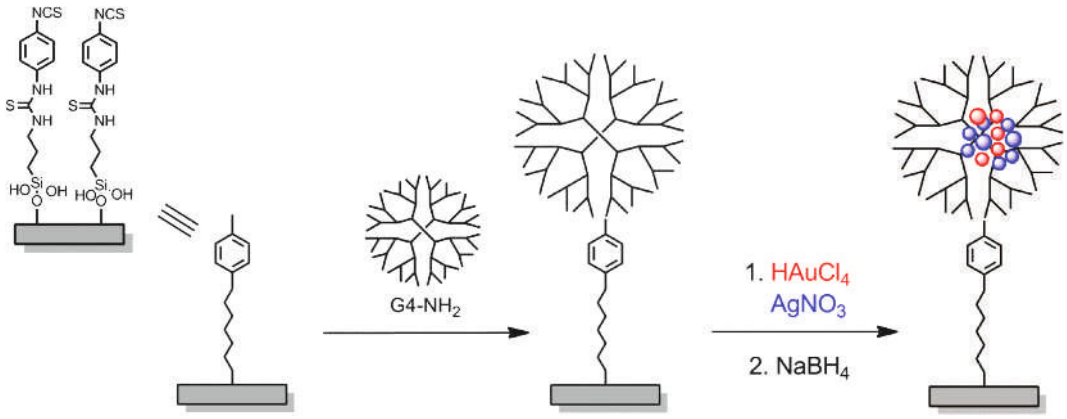

spacing of 2.3 Å was calculated, indicating the (111) lattice plane. This value is almost identical to the one of monometallic Ag and Au, which have similar lattice constants, namely, 4.079 and 4.0765 Å, respectively [21], thus, not allowing a clear distinction between alloy and single metal NPs. Nevertheless, the image shows an excellent atomic alignment within the particle, with no lattice distortion as expected for a homogeneous mixing of Ag and Au. Additionally, energy-dispersive X-ray spectroscopy (EDX) provides powerful information to assess the NP atomic composition. Therefore, several dendrimer–Au/Ag 1:1 nanocomposites were analyzed by EDX. Noteworthy, the values obtained for individual particles match very closely with the feeding atomic composition, the experimental values for Au and Ag being 45.6% and 54.4%, respectively (within a 7% error margin; Figure 2b).

X-ray photoelectron spectroscopy (XPS) provided additional information about the metal composition. The analysis was performed on a silicon dioxide surface functionalized in the same way as the glass microchannel surface. We were particularly interested in the Au/Ag ratio as related to the feed ratios of the two metal salts. Table 1 summarizes the relationship between Ag_{3d} and Au_{4f} peaks for G4-NH_2(Au_xAg_y)-functionalized surfaces, prepared according to the approach depicted in Scheme 1. The results diverge to some extent from the theoretical metal composition. Such behavior may be explained by the

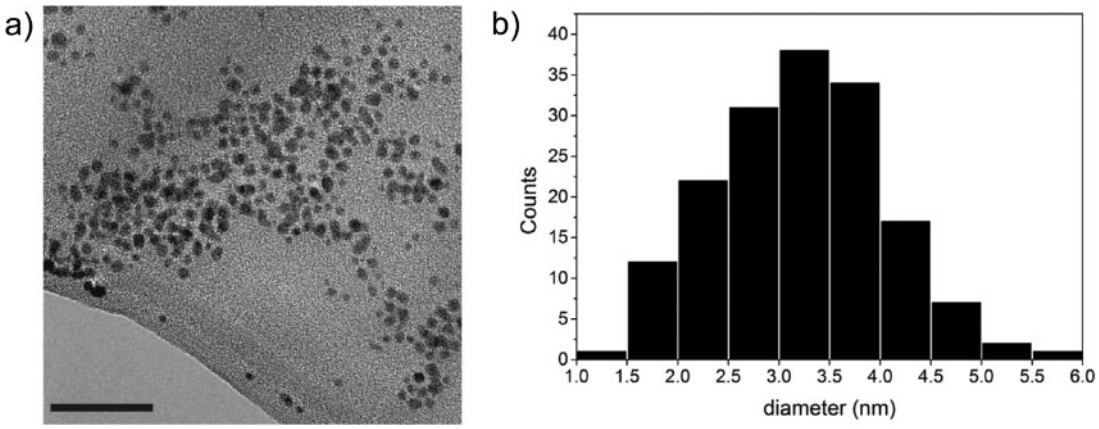

Figure 1. a) TEM image of G4-NH_2 Au/Ag 1:1 NPs (scale bar, 40 nm); b) nanoparticle size distribution

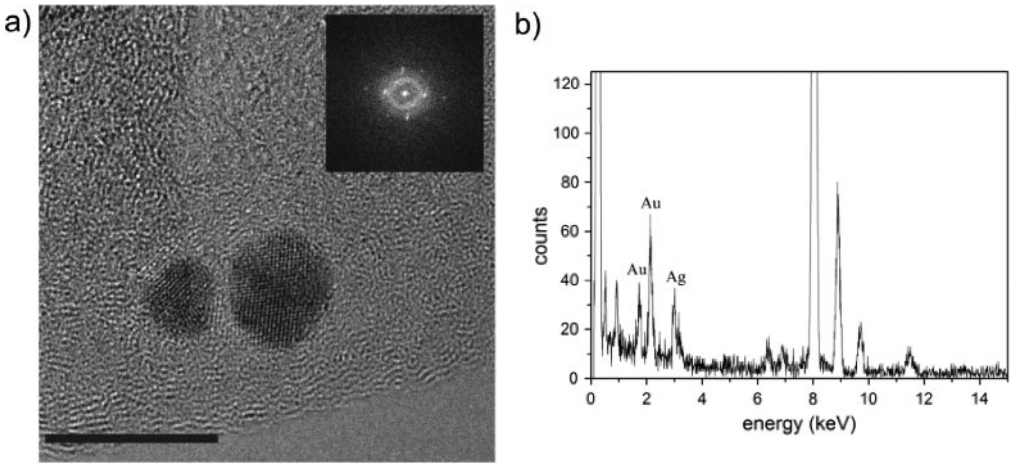

Figure 2. a) HRTEM image of a single crystal of a DEN Au/Ag 1:1 nanocomposite and a Fourier transformed image indicating the electron diffraction pattern in the inset (scale bar, 10 nm). b) EDX spectrum of the DEN Au/Ag 1:1 nanocomposite

Table 1. XPS analysis of the Ag_{3d} and Au_{4f} peaks for a G4-NH_2(Au_xAg_y)-functionalized silicon dioxide surface

Au/Ag	Theoretical	Experimental[a]	Au content (%)
3:1	3	0.67	40
1:1	1	0.42	30
1:3	0.33	0.30	23

[a] Average numbers based on three experiments.

presence of nonspecifically bound metal at the outside of the dendrimer template.

The catalyst loading of a G4-NH_2 1:1 Au/Ag-functionalized microreactor was calculated by total reflection X-ray fluorescence (TXRF). In particular, the amount of both metals retained by the dendrimer templates attached to the microreactor surface was measured, namely, 22 ng (0.11 nmol) of Au and 20 ng (0.18 nmol) of Ag. This confirms the equal loading efficiencies of these metals from a 1:1 feed.

2.2. Influence of Metal Ratio on the Catalytic Reduction of 4-Nitrophenol. The reduction of 4-nitrophenol to 4-aminophenol using $NaBH_4$ was chosen as a model reaction to study the catalytic performance of Au/Ag DEN-functionalized microreactors (Scheme 2). Arguably, the reduction of 4-nitrophenol is one of the most studied reactions for investigating the catalytic activity of metallic NPs and constitutes therefore an optimal benchmark for evaluating the activities of mono- and bimetallic NPs and the efficiencies of their preparation methods [22]. The continuous reaction process was monitored by in-line UV–vis spectroscopy because of the strong absorbance of 4-nitrophenol at 400 nm. The progress of the reaction is characterized by a decrease of the absorbance at 400 nm and a concomitant (small) increase of the absorbance at about 300 nm due to formation of 4-aminophenol (Figure S2) [23].

Furthermore, the overall reaction rate for this reaction appeared to be pseudo-first order when the reducing agent was used in large excess. Therefore, we conducted a kinetic study with the Au/Ag DENs, having different metal ratios as well as pure Au and Ag. An excess of $NaBH_4$ was used to achieve pseudo-first order conditions. At the same reaction conditions ($NaBH_4$ concentration, residence times), only a marginal (<5%) activity was observed in the absence of the catalyst. The kinetic curves shown in Figure 3a represent the activities of the Au/Ag metal ratios employed, namely, 1:0 3:1, 1:1, and 1:3 expressed in terms of nominal Au content (%). For all metal ratios, an induction time of about 15 s could be extrapolated from the kinetic curves. Pure Ag NPs exhibited much longer induction and residence times and their kinetic profile has not been included in Figure 3. In order to quantify the differences in reactivity, the observed rate constants (k_{obs}) were extrapolated from the kinetic curves and plotted versus the amount of gold in the heterometallic NPs (Figure 3b). Strikingly, Au/Ag 1:1 bimetallic nanocomposites gave rise to the highest activity, being remarkably superior to that of other bimetallic feed ratios and to the one of pure gold, which accounts for most of the activity for this reaction.

In fact, as demonstrated by Endo et al. [17], the Au/Ag ratio of DEN bimetallic NPs influences the reaction rate, in which case, the apparent rate constant appeared to be directly proportional to the gold content. The authors speculated that the enhanced catalytic activity that is observed for core–shell and alloy particles is due to an ensemble effect at the surface atoms, although in their study, the maximum of activity was observed for the Au/Ag 3:1 ratio 75% [17, 24]. The k_{obs} for the G4-NH_2 Au/Ag 1:1-functionalized microreactor was of 0.18 s^{-1}, hence, exhibiting a turnover frequency (TOF) of 2850 h^{-1}. Other nanocatalysts have shown TOFs up to 1028 h^{-1}, with only Pd NPs stabilized by a dendritic nanoreactor reaching a value as high as 22,500 h^{-1} [25]. With respect to Au/Ag bimetallic NP catalysts, k_{obs} values of about 0.015 s^{-1} and 0.005 s^{-1} were found in literature at batch scale, thus, confirming the high activity of our catalytic system [26]. Only a G6-OH(Pd_1Cu_1) catalyst showed a similar k_{obs} (0.12 s^{-1}) [22c]. There are only a few examples of metal NPs supported within microfluidic reactors for the reduction of 4-nitrophenol. For instance, the k_{obs} of Ag and Pd NPs entrapped in a brush-functionalized microreactor was of 0.03 s^{-1} [27], lower than in the system presented here.

The improved catalytic efficiency of the Au/Ag DENs, especially in the 1:1 Au/Ag ratio, may be attributed to a combination of electronic and geometric effects (alloy NPs) and the favorable environment of flow microreactors. It is known that, in the case of Au/Ag heterostructures, electrons could transfer from Ag to Au, leading to an increase in the electron density on the surface of the bimetallic heterocomposites [28]. This effect is particularly advantageous for the model reaction under investigation where BH_4^- ions are formed, which in turn interact with the 4-nitrophenol molecule, both adsorbed on the metal surface as demonstrated by the Langmuir–Hinshelwood (LH) model [29]. This aspect was recently confirmed in a study of the reduction of 4-nitrophenol by Ru DENs [30]. It was also demonstrated that, in the presence of various PAMAM-OH carriers, the reduction is not diffusion controlled [30]. However, a slight influence of the dendrimer template was shown by Esumi et al. [31] The rate constant for the reduction of 4-nitrophenol by using dendrimer-stabilized NPs decreased with increasing dendrimer concentration. This is probably due to the coverage of the dendrimer on the metal particle surface, which is avoided with the use of only a single dendrimer layer within the microreactor as in the study presented here.

At last, a continuous-flow investigation was conducted to assess the durability of the catalytic system. Accordingly, a stability study was carried out utilizing the most active catalyst, i.e., the G4-NH_2 Au/Ag 1:1-functionalized microreactor. Satisfyingly, the model reaction could be run for several consecutive days, with only a little decrease of activity upon the 6th day of utilization (Figure 4). The turnover number (TON) for this investigation was 5050 (considering 4 h of continuous process for each day of use). More importantly, the amount of metal leached out of the microreactor in the course of the reaction was only 2 ng as measured by TXRF (corresponding to less than 5% of the total catalyst amount). Interestingly, only Ag was detected, with no trace of Au in the product solution. This aspect can be ascribed to the stabilizing

Scheme 2. Reduction of 4-nitrophenol to 4-aminophenol in Au/Ag DEN-functionalized microreactors

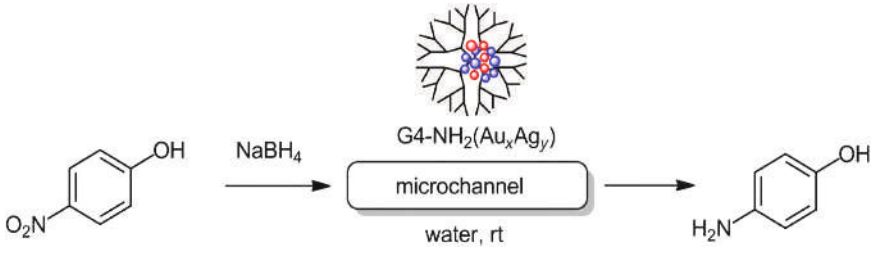

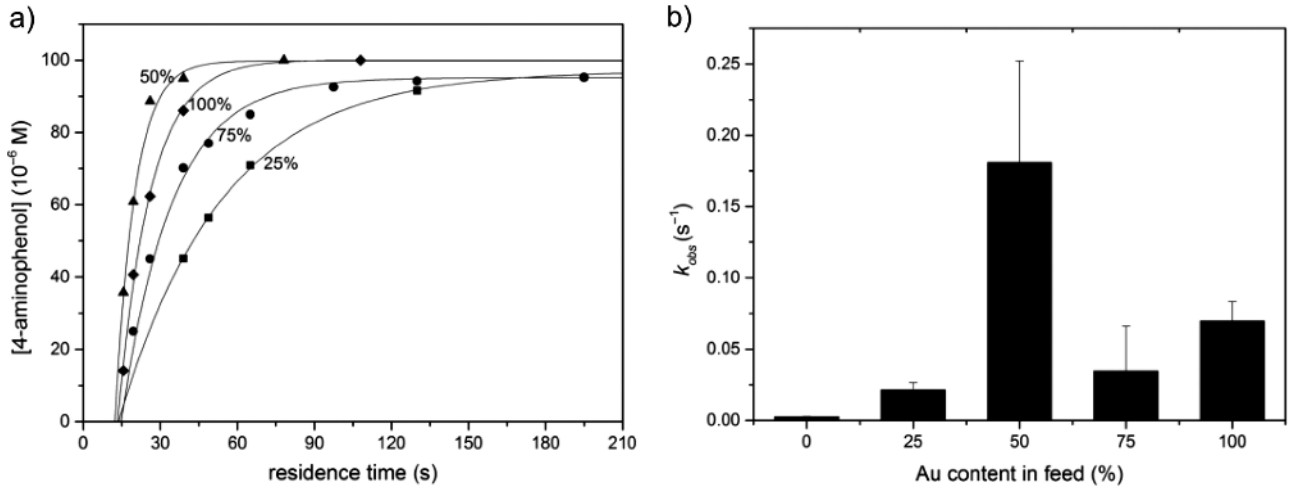

Figure 3. a) Formation of 4-aminophenol versus residence time in G4-NH_2 Au/Ag- and G4-NH_2 Au-functionalized microreactors for different gold contents in the metal feed (%). b) Observed rate constants versus nominal Au content (the error bars represent standard deviations of multiple measurements). [4-Nitrophenol] = 0.1 mM, [$NaBH_4$] = 2 mM, water, rt

effect exerted by the dendrimer template on the metallic nanocomposites, as demonstrated for Pd DENs [14] and witnessed by recent studies of Somorjai and coworkers [32].

3. Conclusions

Alloy Au/Ag DENs were covalently attached to the inner walls of glass microreactors functionalized by means of a reactive monolayer. The bimetallic NPs were formed by cocomplexation of the two metal salts using G4 PAMAM dendrimers as template. The reduction of 4-nitrophenol was chosen as model reaction allowing a kinetic study of different Au/Ag metal ratios. Noteworthy, the Au/Ag 1:1 nanocomposite (TOF of 2850 h^{-1}) performed indisputably better than the other alloy NPs and pure Au, which is the most active metal for the model reaction. The enhanced activity for the 1:1 Au/Ag nanocomposite may be expressed in terms of synergistic effect, geometric and electronic. Finally, the dendrimer template improves the stability of the bimetallic catalyst, as demonstrated by at least six consecutive days of use and minimal metal leaching (5% of the total catalyst amount).

Bimetallic NPs have not yet been fully explored in flow microreactors, with just a few examples in the literature. We envision the increasing importance of this discipline in catalysis, sensing, and electronics, just to name a few. Mechanistic studies of the influence of the type of metals employed and their interaction in alloy or core–shell nanocomposites are needed to further establish this promising research field.

4. Experimental

4.1. Materials and Equipment. The chemicals and solvents were purchased from Sigma-Aldrich unless otherwise stated and were used without purification unless specified. Single-side-polished silicon wafers were purchased from OKMETIC with (100) orientation. Methanol and ethanol (VWR, analytical reagent grade) were used without further purification. Water was purified with the Milli-Q pulse (Millipore, R = 18.2 MΩ cm) ultrapure water system. Toluene was purified through a solvent purification system dispensing ultradry solvents (MBraun, MB-SPS-800). For X-ray photoelectron spectroscopy (XPS), a Quantera Scanning X-ray Multiprobe instrument was used, equipped with a monochromatic Al Kα X-ray source producing approximately 25 W of X-ray power. XPS-data were collected from a surface area of 1000 × 300 μm^2 with a pass energy of 224 eV and a step energy of 0.8 eV for survey scan and 0.4 for high-resolution scans. For quantitative analysis, high-resolution scans were used. Absorption spectra were recorded on a Perkin Elmer Lambda 850 UV–vis spectrometer. The optical path length was 10 mm, and deionized water was used as reference. On-line UV experiments were carried out using a micro-HPLC flow-through cell (ZEUTEC opto-elektronik, Germany), with a spectral UV–Vis–NIR range of 250–2500 nm, an optical path length of 10 mm, and an internal volume of 2 μL. The flow cell is connected, via 2 optical fibers (SR 600 nm, Ocean optics Inc., The Netherlands), to a miniature deuterium halogen light source (DT-Mini-2-GS, Mikropack GmbH, Germany) and to a high-resolution miniature fiber optic spectrometer (HR4000, Ocean optics Inc., The Netherlands). Transmission electron microscopy (TEM) was performed using a Philips CM300 microscope operating at 300 kV. Samples for imaging were deposited onto a 200 mesh copper grid, and the liquid was allowed to dry in air at room temperature. The nanoparticle dimensions were obtained from TEM images with ImageJ software; for each sample, at least 50 particles were measured. Energy-dispersive X-ray spectroscopy (EDX) was performed by a Noran System Six EDX analyzer Nanotrace detector. Total reflection X-ray fluorescence (TXRF) measurements were carried out on a S2-PICOFOX™ (Bruker AXS, Karlsruhe, Germany) system with a low power X-ray tube by means of a Mo source and an energy-dispersive, 50 Peltier-cooled silicon drift detector

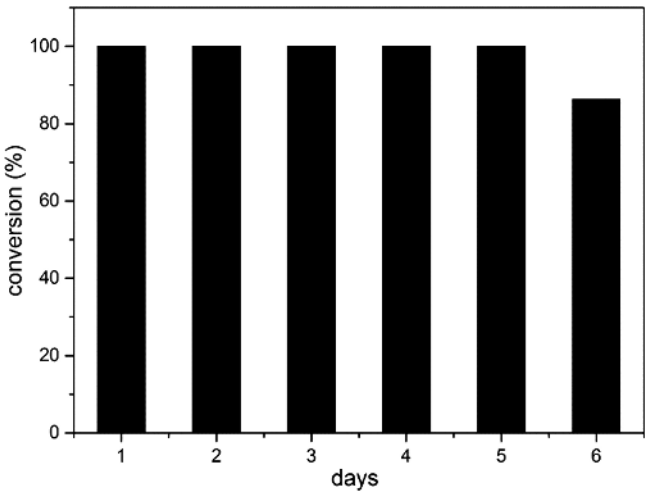

Figure. 4. Conversion versus residence time for the reduction of 4-nitrophenol in a G4-NH_2 Au/Ag 1:1-functionalized microreactor. [4-Nitrophenol] = 0.1 mM, [$NaBH_4$] = 2 mM, water, rt, residence time: 78 s

(SDD, XFlash™). The software SPECTRA version 6.1.5.0 (Bruker AXS, Karlsruhe, Germany) was used for data evaluation.

4.2. Flow Apparatus. In all microreactor experiments, the sample solutions were mobilized by means of a PHD 22/2000 series syringe pump (Harvard Apparatus, United Kingdom) equipped with 500 μL flat tip syringes (Hamilton). Syringes were connected to fused silica capillaries (100 μm i.d., 362 μm o.d., Polymicro Technologies) by means of Upchurch Nanoport™ assembly parts (i.e., Nano-Tight™ unions and fittings, Upchurch Scientific Inc., USA). During the experiments, the microreactor was placed in a home-built chip holder designed for fitting fused silica fibers into the inlet/outlet chip reservoirs by means of commercially available Upchurch Nanoport™ assembly parts. Glass microreactors with a residual volume of 13 μL (dimensions: 150 μm width and 150 μm depth) were purchased from Micronit Microfluidics.

4.3. Functionalization of Flat Silicon Dioxide Surfaces and Microreactor Inner Walls by Dendrimer-Encapsulated Au/Ag Alloy NPs

4.3.1. Deposition of a Monolayer of APTES and DITC. Both the SiO_2 surface and the microreactor channels were cleaned with a Piranha solution (H_2SO_4–H_2O_2 3:1) and then copiously rinsed with water and dried with a stream of nitrogen. (Caution: piranha solution is a very strong oxidant and reacts violently with many organic materials). The clean surface was functionalized with a monolayer of (3-aminopropyl)triethoxysilane (APTES) and *p*-phenylene diisothiocyanate (DITC, Acros Organics) following a slightly modified literature procedure. First, the silicon surface was soaked in a 10-mM solution of APTES in dry toluene for 15 h. For functionalization in the device, the same solution was flowed for 15 h at a flow rate of 0.05 μL min^{-1}. Silicon wafers and microchannels were rinsed with dry toluene and ethanol to remove the unreacted reagent and dried with a stream of nitrogen. Subsequently, the APTES-modified flat surface was reacted with a 50-mM solution of DITC in dry toluene for 5 h. The same solution was flowed within the microreactor for 5 h at 0.05 μL min^{-1}. Silicon wafers and microchannels were rinsed with dry toluene and ethanol to remove the unreacted reagent and dried with a stream of nitrogen.

4.3.2. Formation and Anchoring of G4-NH2(Au_xAg_y), G4-NH2(Au), and G4-NH2(Ag). A methanolic solution of 150 μM G4-NH_2 was reacted with the APTES-DITC-functionalized silicon surface for 10 h at room temperature. After rinsing with methanol and water, the surface was soaked in different 2 mM aqueous solutions of $HAuCl_4$ (Acros Organics) and $AgNO_3$ for 30 min at room temperature. G4-NH_2-enscapsulated Au/Ag alloy NPs were prepared in the following Au/Ag ratios (in 1 mL of water): 1:1 (1×10^{-3} mmol of $HAuCl_4$ and $AgNO_3$), 3:1 (1.5×10^{-3} mmol of $HAuCl_4$ and 0.5×10^{-3} mmol of $AgNO_3$), and 1:3 (0.5×10^{-3} mmol of $HAuCl_4$ and 1.5×10^{-3} mmol of $AgNO_3$). For pure Au and Ag NPs, 2×10^{-3} mmol of $HAuCl_4$ and $AgNO_3$ were added to 1 mL of water, respectively. Afterwards, the reduction of the metallic particles was obtained by reaction with a 20-mM aqueous solution of $NaBH_4$ (20 min). The same procedure was followed for the microreactor functionalization by flowing the dendrimer, gold and silver salts, and reducing agent solutions at 0.05 μL min^{-1} for the respective times.

4.4. Continuous-Flow Reduction of 4-Nitrophenol. 4-Nitrophenol (0.1 mM) was mixed with a freshly prepared solution of $NaBH_4$ (2 mM) in water. This solution was passed through the catalytic microreactors at different flow rates, and the reaction was monitored by in-line UV–vis spectroscopy. The decrease of the 4-nitrophenol absorbance at 400 nm was used to calculate the pseudo-first order rate constants for the different DEN-functionalized microreactors. The turnover frequency (TOF) for the G4-NH_2 1:1 Au/Ag-functionalized microreactor was calculated based on the moles of product per unit time per moles of catalyst within the microreactor volume (13 μL). The moles of catalyst are based on the total amount of metal atoms (0.11 nmol of Au and 0.18 nmol of Ag). The observed rate constant was used in the calculation according to the formula: $(k_{obs} * M_{product} * V_{microreactor})/(mol_{cat} * 3600)$.

Acknowledgements. We gratefully acknowledge the Netherlands Organization for Scientific Research (NWO) for financial support (project ECHO.09.TD.024). Michael Holtkamp and Uwe Karst are gratefully thanked for their help with the TXRF measurements.

Supporting Information

Electronic Supplementary Material (ESM) is available in the online version at doi: 10.1556/1846.2015.00018.

References

1. (a) Notar Francesco, I.; Fontaine-Vive, F.; Antoniotti, S. *ChemCatChem* **2014**, *6*, 2784–2791; (b) Singh, A. K.; Xu, Q. *ChemCatChem* **2013**, *5*, 652–676; (c) Shan, S.; Luo, J.; Yang, L.; Zhong, C.-J. *Catal. Sci. Technol.* **2014**, *4*, 3570–3588; (d) Tao, F. *Chem. Soc. Rev.* **2012,** *41*, 7977–7979.

2. Dai, Y.; Wang, Y.; Liu, B.; Yang, Y. *Small* **2015**, *11*, 268–289.

3. (a) Kalidindi, S. B.; Jagirdar, B. R. *ChemSusChem* **2012**, *5*, 65–75; (b) Polshettiwar, V.; Varma, R. S. *Green Chem.* **2010**, *12*, 743–754.

4. (a) Sankar, M.; Dimitratos, N.; Miedziak, P. J.; Wells, P. P.; Kiely, C. J.; Hutchings, G. J. *Chem. Soc. Rev.* **2012**, *41*, 8099–8139; (b) Gao, F.; Goodman, D. W. *Chem. Soc. Rev.* **2012**, *41*, 8009–8020.

5. Ferrando, R.; Jellinek, J.; Johnston, R. L. *Chem. Rev.* **2008**, *108*, 845–910.

6. Jiang, H.-L.; Xu, Q. *J. Mater. Chem.* **2011**, *21*, 13705–13725.

7. Na, K.; Zhang, Q.; Somorjai, G. *J. Clust. Sci.* **2014**, *25*, 83–114.

8. (a) Myers, V. S.; Weir, M. G.; Carino, E. V.; Yancey, D. F.; Pande, S.; Crooks, R. M. *Chem. Sci.* **2011**, *2*, 1632–1646; (b) Astruc, D.; Boisselier, E.; Ornelas, C. *Chem. Rev.* **2010**, *110*, 1857–1959.

9. (a) Chandler, B.; Gilbertson, J. In *Dendrimer Catalysis*; Gade, L., Ed.; Springer Berlin Heidelberg, 2006; Vol. 20, pp. 97–120; (b) Peng, X.; Pan, Q.; Rempel, G. L. *Chem. Soc. Rev.* **2008**, *37*, 1619–1628.

10. (a) Scott, R. W. J.; Wilson, O. M.; Oh, S.-K.; Kenik, E. A.; Crooks, R. M. *J. Am. Chem. Soc.* **2004**, *126*, 15583–15591; (b) Scott, R. W. J.; Sivadinarayana, C.; Wilson, O. M.; Yan, Z.; Goodman, D. W.; Crooks, R. M. *J. Am. Chem. Soc.* **2005**, *127*, 1380–1381; (c) Peng, X.; Pan, Q.; Rempel, G. L.; Wu, S. *Catal. Commun.* **2009**, *11*, 62–66.

11. (a) Zhang, Y. T.; Arancon, R. A. D.; Lam, L. Y. F.; Luque, R. *Chem. Today* **2014**, *32*, 36–39; (b) Obermayer, D.; Balu, A. M.; Romero, A. A.; Goessler, W.; Luque, R.; Kappe, C. O. *Green Chem.* **2013**, *15*, 1530–1537; (c) Gross, E.; LiuJack, H.-C.; Toste, F. D.; Somorjai, G. A. *Nat. Chem.* **2012**, *4*, 947–952.

12. (a) Rebrov, E. V.; Klinger, E. A.; Berenguer-Murcia, A.; Sulman, E. M.; Schouten, J. C. *Org. Process Res. Dev.* **2009**, *13*, 991–998; (b) Mimura, N.; Hiyoshi, N.; Fujitani, T.; Dumeignil, F. *RSC Adv.* **2014**, *4*, 33416–33423; (c) Moitra, N.; Kanamori, K.; Ikuhara, Y. H.; Gao, X.; Zhu, Y.; Hasegawa, G.; Takeda, K.; Shimada, T.; Nakanishi, K. *J. Mater. Chem. A* **2014**, *2*, 12535–12544.

13. (a) Munirathinam, R.; Huskens, J.; Verboom, W. *Adv. Synth. Cat.* **2015**, 357, 1093–1123; (b) Wiles, C.; Watts, P. *Green Chem.* **2014**, *16*, 55–62; (c) Elvira, K. S.; i Solvas, X. C.; Wootton, R. C. R.; deMello, A. J. *Nat. Chem.* **2013**, *5*, 905–915; (d) Newman, S. G.; Jensen, K. F. *Green Chem.* **2013**, *15*, 1456–1472; (e) Xu, B.-B.; Zhang, Y.-L.; Wei, S.; Ding, H.; Sun, H.-B. *ChemCatChem* **2013**, *5*, 2091–2099; (f) Frost, C. G.; Mutton, L. *Green Chem.* **2010**, *12*, 1687–1703.

14. Ricciardi, R.; Huskens, J.; Holtkamp, M.; Karst, U.; Verboom, W. *ChemCatChem* **2015**, *7*, 936–942.

15. Ricciardi, R.; Huskens, J.; Verboom, W. *Org. Biomol. Chem.* **2015**, *13*, 4953–4959.

16. Ludden, M. J. W.; Ling, X. Y.; Gang, T.; Bula, W. P.; Gardeniers, H. J. G. E.; Reinhoudt, D. N.; Huskens, J. *Chem. Eur. J.* **2008**, *14*, 136–142.

17. Endo, T.; Yoshimura, T.; Esumi, K. *J. Colloid Interface Sci.* **2005**, *286*, 602–609.

18. (a) Wilson, O. M.; Scott, R. W. J.; Garcia-Martinez, J. C.; Crooks, R. M. *J. Am. Chem. Soc.* **2004**, *127*, 1015–1024; (b) Link, S.; Wang, Z. L.; El-Sayed, M. A. *J. Phys. Chem. B* **1999**, *103*, 3529–3533.

19. Mallin, M. P.; Murphy, C. J. *Nano Lett.* **2002**, *2*, 1235–1237.

20. Chung, Y.-M.; Rhee, H.-K. *Catal. Lett.* **2003**, *85*, 159–164.

21. (a) Davey, W. P. *Phys. Rev.* **1925**, *25*, 753–761; (b) Shin, Y.; Bae, I.-T.; Arey, B. W.; Exarhos, G. J. *J. Phys. Chem. C* **2008**, *112*, 4844–4848.

22. (a) Wunder, S.; Lu, Y.; Albrecht, M.; Ballauff, M. *ACS Catal.* **2011**, *1*, 908–916; (b) Esumi, K.; Miyamoto, K.; Yoshimura, T. *J. Colloid Interface Sci.* **2002**, *254*, 402–405; (c) Pozun, Z. D.; Rodenbusch, S. E.; Keller, E.; Tran, K.; Tang, W.; Stevenson, K. J.; Henkelman, G. *J. Phys. Chem. C* **2013**, *117*, 7598–7604.

23. (a) Lee, J.; Park, J. C.; Song, H. *Adv. Mater.* **2008**, *20*, 1523–1528; (b) Panigrahi, S.; Basu, S.; Praharaj, S.; Pande, S.; Jana, S.; Pal, A.; Ghosh, S. K.; Pal, T. *J. Phys. Chem. C* **2007**, *111*, 4596–4605.

24. Liu, P.; Norskov, J. K. *Phys. Chem. Chem. Phys.* **2001**, *3*, 3814–3818.

25. (a) Deraedt, C.; Salmon, L.; Astruc, D. *Adv. Synth. Cat.* **2014**, *356*, 2525–2538; (b) Holden, M. S.; Nick, K. E.; Hall, M.; Milligan, J. R.; Chen, Q.; Perry, C. C. *RSC Adv.* **2014**, *4*, 52279–52288.

26. (a) An, Q.; Yu, M.; Zhang, Y.; Ma, W.; Guo, J.; Wang, C. *J. Phys. Chem. C* **2012**, *116*, 22432–22440; (b) Jiang, H.-L.; Akita, T.; Ishida, T.; Haruta, M.; Xu, Q. *J. Am. Chem. Soc.* **2011**, *133*, 1304–1306.
27. Costantini, F.; Benetti, E. M.; Tiggelaar, R. M.; Gardeniers, H.; Reinhoudt, D. N.; Huskens, J.; Vancso, G. J.; Verboom, W. *Chem. Eur. J.* **2010**, *16*, 12406–12411.
28. (a) Xia, B.; He, F.; Li, L. *Langmuir* **2013**, *29*, 4901–4907; (b) Wunder, S.; Polzer, F.; Lu, Y.; Mei, Y.; Ballauff, M. *J. Phys. Chem. C* **2010**, *114*, 8814–8820.
29. Xu, W.; Kong, J. S.; Chen, P. *J. Phys. Chem. C* **2009**, *113*, 2393–2404.
30. Antonels, N. C.; Meijboom, R. *Langmuir* **2013**, *29*, 13433–13442.
31. Esumi, K.; Isono, R.; Yoshimura, T. *Langmuir* **2003**, *20*, 237–243.
32. Li, Y.; Liu, J. H.-C.; Witham, C. A.; Huang, W.; Marcus, M. A.; Fakra, S. C.; Alayoglu, P.; Zhu, Z.; Thompson, C. M.; Arjun, A.; Lee, K.; Gross, E.; Toste, F. D.; Somorjai, G. A. *J. Am. Chem. Soc.* **2011**, *133*, 13527–13533.